Published in final edited form as:
*Bioconjug Chem*. 2012 April 18; 23(4): 671–682. doi:10.1021/bc200264c.

# Nanoparticles labeled with Positron Emitting Nuclides: Advantages, Methods, and Applications

**Yongjian Liu*** and **Michael J. Welch**
Department of Radiology, Washington University in St. Louis, MO 63110

## Abstract

Over the past decade, positron emitter labeled nanoparticles have been widely used in and substantially improved for a range of diagnostic biomedical research. However, given growing interest in personalized medicine and translational research, a major challenge in the field will be to develop disease specific nanoprobes with facile and robust radiolabeling strategies and that provide imaging stability, enhanced sensitivity for disease early stage detection, optimized *in vivo* pharmacokinetics for reduced non-specific organ uptake, and improved targeting for elevated efficacy. This review briefly summarizes the major applications of nanoparticles labeled with positron emitters for cardiovascular imaging, lung diagnosis and tumor theranostics.

## INTRODUCTION

During the last decade, molecular imaging has expanded due to its unique suitability to support personalized medicine by using modified or engineered molecules that can reveal individual biology when coupled with an appropriate imaging approach. Molecular imaging approaches include both single modality such as positron emission tomography (PET), single photon emission computed tomography (SPECT), magnetic resonance imaging (MRI), magnetic resonance spectroscopy (MRS), computed tomography (CT), ultrasound, bioluminescence, and fluorescence imaging, and also multimodalities, such as PET/CT, SPECT/CT and PET/MR.[1] Among these approaches, the radionuclide-based imaging methods, especially PET, have been a particular focus in biomedical research due to advantages that include high sensitivity (picomolar level) and limitless tissue penetration.[2]

While many types of molecules have been used in molecular imaging, a growing area of interest is the use of nanoparticles, which have great potential for early detection, accurate diagnosis, and personalized therapy of various diseases, especially cancer.[3] Nanoparticles are structures ranging in size from 1 to100 nm (Figure 1). Nanoparticles show unique size-dependent physical and chemical properties, which can be optical, magnetic, catalytic, thermodynamic, and electrochemical. [4] Generally, nanoparticles used for biomedical research can be categorized into three groups: 1) inorganic nanoparticles including quantum dots, iron oxide nanoparticles, gold nanostructures, and upconversion nanophosphors; 2) polymer nanoparticles such as core-shell dendrimers and amphiphilic nanoparticles; 3) lipid nanoparticles including liposomes and solid lipid nanoparticles. Additionally, radiolabeled carbon nanotubes and nanodiamonds have also been widely explored for oncological applications. [5–8] Nanoparticles' pharmacokinetics and biodistribution have been reviewed in detail elsewhere. [9, 10]

Corresponding author: Yongjian Liu, Ph.D., Department of Radiology, Washington University, Campus Box 8225, 510 S. Kingshighway Blvd., St. Louis, MO 63110. liuyo@mir.wustl.edu, Phone: 314-362-8431, Fax: 314-362-9940.

Nanoparticles' design flexibility enables tunable *in vivo* pharmacokinetics to improve delivery efficacy and to reduce non-specific organ uptake by varying the size, charge, and surface modification. [11] With a diameter about 100nm, nanoparticles show prolonged blood circulation and relatively low rate of mononuclear phagocyte system (MPS) uptake. [10] Their size also fills a critical position between the macroscopic world and molecular-level detail, and they can be designed to provide unique advantages over both macroscopic materials and molecular systems. Because their size is comparable to large biological molecules (antibodies, DNA), nanoparticles can be designed to interact with various biomolecules both on the surface and inside cells, leading to significantly improved diagnosis and treatment efficacy.[3] Another noteworthy physicochemical characteristic is the nanoparticle's high surface area to volume ratio, which enables rich surface chemistry for various targeting components while retaining high loading capacity for detection elements and therapeutic payload, as well as multifunctionality for synergistic applications (Figure 1).[12] Regarding charge, neutral nanoparticles are reported to demonstrate a slow clearance profile and reduced hepatic and splenic accumulations compared to charged nanoparticles,[13] while positively charged nanoparticles administered intravenously often form aggregates due to the presence of negatively charged serum proteins.[14] To reduce opsonization and aggregation caused by protein deposition, hydrophilic polymers such as polyethylene glycol are normally grafted onto the surface of nanoparticles, which also improves blood retention for optimized targeting and delivery. [15]

Over the last decade, growth in the applications of nanoparticles in molecular imaging and drug delivery by utilizing gamma-emitting radioisotopes and positron emitters [16–21] has led to drug discovery and numerous clinical trials. [22–25] Due to broad application of PET isotopes in translational research, we focus on the major biomedical applications of nanoparticles radiolabeled with these positron emitters. [26–30]

## APPLICATIONS OF PET RADIONUCLIDE LABELED NANOPARTICLES

PET radionuclide labeled nanoparticles have been extensively used in both preclinical and clinical studies as a tool to explore nanoparticles' *in vivo* pharmacokinetics, imaging capability, and theranostic potential. [19, 22, 31, 32] For nanoparticles with different physicochemical properties and functional groups, the specific PET isotope and radiolabeling strategy need to be carefully considered to generate an optimal imaging outcome. The nuclear characteristics of commonly used PET radionuclides for nanoparticles are summarized in Table 1.

There are two main radiolabeling strategies for nanoparticles. One is to radiolabel the nanoparticle structure itself, either on the surface or in the core. The other approach is to radiolabel the payload encapsulated inside the nanoparticle. These two approaches share much of their chemistry and are both widely used for nanoparticle radiolabeling (Table 2). [33]

In designing a radiolabeled nanoparticle for biomedical applications, some key factors need to be considered. The first of these is radiolabeling integrity. For *in vitro* or *in vivo* applications of radiolabeled nanoparticles, the radionuclide itself is observed or detected rather than the nanoparticle or the payload. Thus the nanoparticle structure and radiolabeling strategy must both be designed to get robust, stable radiolabeling. The second factor to consider is application compatibility – the half-life of the radionuclide needs to be congruent with the binding kinetics of the probe and target, as well as the probe's *in vivo* pharmacokinetics. A third factor is the targeting efficiency and radiolabeling specific activity, since a well-designed nanoparticle that allows increased loading of targeting ligands and high radiolabeling specific activity can provide elevated binding efficiency and

reduce the required administration of nanoparticle to just trace amounts. The fourth factor is translational capability, since the U. S. Food and Drug Administration (FDA) approval for human application will be needed to explore the clinical potential of nanoparticles. For example, although there are chelators showing better $^{64}$Cu radiolabeling stability for PET imaging,[34] DOTA (1,4,7,10-tetraazacyclododecane-1,4,7,10-tetraacetic acid) is still the most used chelator for translational research owing to its FDA approval and wide applications in clinical trials. [35]

A wide range of nanoparticles have been labeled with a variety of radionuclides. Quantum dots (QDs) are inorganic fluorescent semiconductor nanoparticles with desirable properties for optical imaging applications and have been radiolabeled with various radionuclides to explore their *in vivo* pharmacokinetics in an effort to develop multifunctional imaging probes. However, the hydrophobic nature of QDs leads to short blood circulation and insufficient targeting even after surface pegylation. [13, 36] More importantly, their potential toxicity limits the translational application of QDs.[37] Magnetic nanoparticles, especially iron oxide nanoparticles have also been widely explored for imaging applications because of high $T_2$ relaxivity for enhanced contrast, none radiation burden, biocompatibility and low clinical toxicity. [38, 39] In addition, although most applications of iron nanoparticles have been focused on developing MRI contrast agents, preparation of iron oxide based PET/MR dual functional nanoparticles has been an active research area. So far, various radiolabeling strategies with different positron emitters including $^{64}$Cu, $^{68}$Ga and $^{124}$I have been used to study the *in vivo* biodistribution profile and targeting efficiency of iron oxide nanoparticles with high radiolabeling yields and specific activities in a variety of animal disease models. [26, 40–42] Another target is gold nanostructures, which have tunable optical properties in the near-infrared (NIR) region (650 to 900 nm) and are thus particularly attractive for hyperthermia based on the photothermal effect, leading to increased cancer theranostic applications. [9, 43] Of the available imaging modalities, PET is the most widely used technique to monitor the delivery of gold nanostructures due to its high sensitivity and quantitative detection. A recent study of a $^{64}$Cu-radiolabeled gold nanoshell showed clear tumor uptake, indicating the potential for not only PET imaging but also as a theranostic agent. [44]

Polymer nanoparticles have been widely used for biomedical imaging applications using a variety of radiolabeling strategies due to the versatility of synthetic chemistry. The structural design and *in vivo* PET imaging of polymer nanoparticles is reviewed in detail elsewhere. [17] In addition, liposome nanoparticles have been used for drug delivery since their initial discovery 40 years ago and are available with a myriad of possible compositions and modifications. [45] Significant progress has been achieved by utilizing liposomes as nanocarriers for both diagnosis and therapy. A wide variety of radionuclides and labeling strategies have been employed for generating radioactive liposomes, and these are reviewed elsewhere. [46]

Silica nanoparticles, due to the well-known biocompatibility, have also been explored for various biomedical applications with radiolabels. [47, 48] With $^{18}$F labeling, the thermally hydrocarbonized porous silicon nanoparticle demonstrated that the particles passed intact through the gastrointestinal tract after oral administration and were not absorbed from a subcutaneous deposit. With intravenous injection, a fast MPS clearance profile was confirmed. This silica nanoparticle exhibited excellent *in vivo* stability, low cytotoxicity, and non-immunogenic profiles, indicating the potential for oral drug delivery. [47] In another study, an organically modified silica nanoparticle also showed no toxicity *in vivo* and full clearance through hepatobiliary excretion, which was confirmed by both $^{124}$I and near infrared dye DY776 labeling. [48] Lately, nanodiamonds have also been proposed as a promising biomaterial for drug delivery owning to the biocompatibility of this form of

carbon. [49] With $^{18}F$ radiolabeling, these nanodiamonds showed high lung, liver and spleen uptake, and significant excretion through the urinary tract. [7] Another recently emerged nanostructure for oncological applications is known as an upconversion nanoparticle. This nanostructure has very fast radiofluorination kinetics and multimodality imaging properties, but its *in vivo* pharmacokinetics still need improvement to achieve sufficient blood circulation. [50–52]

With increasing support from the National Institute of Health to study and develop nanotechnology, [53] additional applications of nanomedicine research is expected. Here we describe selected applications of radiolabeled nanoparticles with the focus on core-shell polymeric nanoparticles.

## Radiolabeled nanoparticles for cardiovascular imaging

It is well known that systemically administered nanoparticles tend to be sequestered by the MPS system and to accumulate mainly in the liver and spleen. Clearance from the bloodstream depends on particle size, surface configuration, and several other factors, and the first step is opsonization that triggers complement activation and macrophage recognition.[54] To target the low abundance biomarkers in animal cardiovascular disease models, nanoparticles must have high radiolabeling specific activity and binding specificity and be able to circulate for a sufficient period of time in the bloodstream, which requires well-defined structure, composition, and controlled *in vivo* properties. Among various nanostructures (such as iron oxide, silica, and gold nanoparticles), [55–59] amphiphilic core-shell nanostructures have received particular attention because of the tunable *in vivo* pharmacokinetics and versatile conjugation chemistry. [60, 61] Shell cross-linked knedel-like nanoparticles (SCKs) are comprised of a hydrophobic polystyrene core that can be used to load hydrophobic drug molecules, and a hydrophilic external shell of poly (acrylic acid-co-acrylamide) that provides additional sites for other functional units such as imaging moieties. Through various synthetic strategies, especially cross-linking, SCKs can be prepared with controlled size, surface charge, pegylation density, multi-functionality, and tuned *in vivo* pharmacokinetics. [54, 62] Additionally, the multivalency of SCKs empowers flexible radiochemistry ($^{64}Cu$, $^{76}Br$, $^{124}I$, and $^{18}F$) for PET applications. By conducting DOTA conjugation before nanoparticle assembly, the amount of DOTA accessible for $^{64}Cu$ labeling could be accurately controlled with more than 400 copies per SCK, leading to a specific activity greater than $1.48\times10^7$ Bq/μg.[63]

Another type of core-shell star-like or comb-like co-polymer could be prepared with nitroxide mediated living radical polymerization to create defined sizes and morphologies. In one example, the chelator DOTA was placed in an internal, hydrophilic environment allowing efficient $^{64}Cu$ radiolabeling to make a protected and high specific activity nanoscopic imaging probe. Biodistribution studies showed a distinct correlation between the length of PEG grafts and the *in vivo* circulation time; with increased PEG chain length, increased blood retention and reduced MPS system uptake were observed.[64] Furthermore, the cargo loading capacity of this type of nanoparticle can be adjusted while retaining similar physicochemical properties. In a recent study, varying amounts of RGD peptide (5%-50% RGD) were accurately conjugated to the shell of comb-like nanoparticles for targeting $\alpha_v\beta_3$ integrin, and these RGD-combs all maintained similar sizes and radiolabeling specific activities. [65, 66] The *in vitro* studies of the RGD-combs showed positive correlation between RGD peptide loading and uptake in $\alpha_v\beta_3$ integrin-positive U87MG glioblastoma cells, demonstrating the importance of controlled conjugation of targeting groups to achieve optimal targeting performance with multivalent nanoparticle systems. [66] Further, the comb nanoparticles were conjugated with C-type atrial natriuretic factor (CANF) to target the natriuretic peptide clearance receptor (NPRC) in a mouse angiogenesis model. By controlling the number of DOTA conjugation, high specific activity (5.4±1.2GBq/nmol)

of $^{64}$Cu radiolabeling could be achieved, ensuring the trace administration of $^{64}$Cu-DOTA-CANF-comb (7 pmol) for imaging studies. PET images showed significantly higher standardized uptake values (SUVs) at angiogenesis sites created by hindlimb ischemia compared to contralateral control sites. More importantly, the SUVs of $^{64}$Cu-DOTA-CANF-comb were 3.4 times higher than those obtained with DOTA-CANF peptide tracer and about triple of those from the non-targeted $^{64}$Cu-DOTA-comb, demonstrating the superiority of a multivalent nanoprobe over the corresponding monovalent CANF peptide for *in vivo* molecular targeting, (Figure 2).[67]

In developing nanoparticles for targeted drug delivery, controlled release kinetics, bioavailability and reduced toxicity are key considerations, which have made biodegradable nanoparticles an active research area. [68–70] Compared to the inorganic nanoparticles, the polymeric nanoparticles can be uniquely prepared with biodegradable core or crosslinker for programmed release of therapeutic payload through enzyme or pH response degradation (Figure 3), which greatly enhances their biocompatibility and makes them better candidates for targeted diagnosis and drug delivery. Thus, a core-shell biodegradable dendritic nanoprobe labeled with $^{76}$Br has been prepared for targeting $\alpha_v\beta_3$ integrins expressed in a mouse angiogenesis model. The controlled introduction of targeting CRGDC peptide to the shell offered 50-fold enhancement of *in vitro* binding affinity to $\alpha_v\beta_3$ integrins relative to the monovalent RGD peptide alone. *In vivo*, specific targeting to $\alpha_v\beta_3$ was observed with the targeted nanoprobe demonstrating a 6-fold increase of receptor-mediated endocytosis at the injured site compared to the control nanoprobe (Figure 4).[27] Additionally, the potential of poly(lactide-co-glycolide) based biodegradable nanoparticles have also been assessed for PET imaging due to their FDA approval for human use. [71]

Iron oxide nanoparticles have been widely used in cardiovascular imaging with various radiolabels. With carbohydrates such as dextran coating and diethylenetriaminepentaacetic acid (DTPA) conjugation, the $^{64}$Cu radiolabeled iron oxide nanoparticle ($^{64}$Cu-TNP) was used to target macrophage in an apolipoprotein E deficient (apoE$^{-/-}$) mouse model of aneurysms. The high specific activity ($3.7\times10^8$ Bq/mg Fe of nanoparticle) ensured lower dose administration (1.5 mg Fe/kg body weight) than that used in oncology clinical trials (2.6 mg Fe/kg body weight) and sensitive detection of nanoparticle accumulation in various organs. The *in vivo* biodistribution of $^{64}$Cu-TNP showed sufficient blood circulation ($t_{1/2} \geq$ 4h) and major accumulation in liver and intestine. PET/CT imaging clearly showed the significant localization of $^{64}$Cu-TNP in the thoracic aorta with a target-to-background ratio of 5.1±0.9, indicating the clinical translatability of this radiolabeled nanoparticle. Furthermore, an $^{18}$F radiolabeled iron oxide nanoparticle ($^{18}$F-CLIO) has been developed due to the wide availability, sensitivity, and covalent radiolabeling of this radioisotope.[72] With rapid [$^{18}$F] click fluorination, high radiolabeling efficiency and specific activity were achieved ($6.8 \pm 0.8 \times 10^8$ Bq/mg Fe of nanoparticle). The *in vivo* pharmacokinetics studies showed comparable blood retention to the $^{64}$Cu-TNP. In the apoE$^{-/-}$ aneurysms mouse model, PET imaging showed that the avid internalization by phagocytic cells led to significantly higher tracer accumulation at aneurysms relative to wild-type aorta.[73]

## Radiolabeled nanoparticles for lung imaging

The incidence of respiratory disease and infections such as asthma, chronic obstructive pulmonary disease, cystic fibrosis, infectious disease, and tuberculosis is increasing worldwide. The classification of chronic respiratory diseases as a major disease burden by the World Health Organization has led to increased efforts to prevention, diagnosis and treatment of these diseases.[74] The current challenges for respiratory disease treatment include the sustained delivery and controlled release of drugs, reduction of side effects caused by high dose administration, and increasing drug resistance. Nanotechnology-based delivery systems have gained attention for use in pulmonary diagnosis and therapy due to

their capacity for targeted deposition, bioadhesion, bioavailability, and biocompatibility, and their sustained release, which allows reduced dosing frequency and improves convenience for the patient.[75] So far, a variety of nanocarriers have been used for pulmonary applications including liposomes, solid lipid nanoparticles, metal nanoparticles, nanotubes, and polymeric nanoparticles.[76, 77] Among these nanostructures, owing to the concern about the toxicity, those with potential clinical pulmonary applications such as polymeric nanoparticles, especially the ones made from biodegradable materials have been an active area in both lung diagnosis and treatment.[78]

Recently, various materials such as poly(lactide-co-glycolide), polyacrylates, and polyacrylamide have been used for formulation of biodegradable nanoparticles. [75, 76, 79, 80] In contrast to the hydrophobic materials, the polyacrylamide based hydrogel offers excellent biocompatibility and hydrophilicity. It also is strongly endosome-disrupting, which makes it a candidate for the cytoplasmic delivery/imaging. [81, 82] With an acid-degradable crosslinker, the entrapped payload can be released in a pH-dependent manner inside endosomes. [83] In addition, for better cellular delivery, a cell penetration peptide (CPP) can be used on the nanoparticles to get various cargos into the cells without disturbing the stability of the cell membrane and with low cytotoxic effects. [84] In a recent study, it was reported that the optimal size for deposition in the deep lung for systemic delivery is approximately 1–3μm – microparticles rather than nanoparticles. [85] Therefore, a nona-arginine functionalized polyacrylamide-based microparticle was synthesized to study the delivery efficiency of entrapped protein into non-phagocytic lung epithelial cells (BEAS-2B). *In vitro* results showed effective delivery of encapsulated BSA-Alexa Fluor 488 into the BEAS-2B cells in both CPP- and concentration-dependent manners, as well as a time dependency. [86] As a result, this CPP-modified microparticle was labeled with radiohalogens ($^{125}$I and $^{76}$Br) for animal studies to assess the *in vivo* fate, lung retention, and cellular uptake after intratracheal administration. Furthermore, nanosized CPP particles were also synthesized to compare size-related differences in the clearance profiles. The biodistribution studies revealed that particle retention and extrapulmonary distribution was, in part, size dependent. Microparticles were rapidly cleared by mucociliary routes but, unexpectedly, also through circulation. In contrast, nanoparticles had prolonged lung retention enhanced by the CPP, which was confirmed by the PET imaging analysis with $^{76}$Br-radiolabeled nanoparticles (Figure 5). The studies indicate the potential of microparticles for short-term applications and benefits of nanoparticles for serial imaging or therapy of a persistent lung injury. [29] In contrast, a study of acute lung injury used latex nanoparticles coated with anti-intercellular adhesion molecule-1(ICAM-1) antibody and labeled with $^{64}$Cu for targeting the pulmonary endothelium. Biodistribution studies showed 3- to 4-fold higher uptake in the lungs of mice injected with ICAM-targeted nanoparticles than those receiving control nanoparticles. PET imaging clearly demonstrated the accumulation of radioactivity in the lungs. However, metabolic studies showed that the *in vivo* stability of this nanoprobe needs further improvement for prolonged pulmonary drug delivery. [28]

Lately, a new type of promising biomaterial-carbon known as a nanodiamond has been explored for biomedical applications due to its biocompatibility, ability to cross the cell membrane, and capability to be functionalized to act as carriers. The initial biodistribution and PET imaging via $^{18}$F radiolabeling showed high pulmonary retention, most likely by size exclusion, indicating potential for lung applications. [87] Clinically, $^{68}$Ga-labeled carbon nanoparticles have also been used for pulmonary embolism PET/CT ventilation-perfusion imaging and has demonstrated its superiority to conventional V/Q lung scintigraphy. [88]

## Radiolabeled nanoparticles for tumor imaging

One hundred years ago, Paul Ehrlich proposed the idea of “magic bullet” for the development of medicine to specifically target the cancer disease. [89] Recently, development

of molecular biology and genetic research, two major antitumor strategies have been revealed: 1) utilization of molecularly targeted therapeutics to block hallmarks of cancer, and 2) development of novel drug delivery systems utilizing tumor-specific nanomedicines to improve the pharmacokinetics and bioavailability of vehicle-carried drugs. [90] Because of the versatile physiochemical properties of the nanostructure, in contrast to conventional anti-cancer drugs, nanoparticles can provide significant improvements in pharmacokinetics, targeting specificity and efficiency, diagnostic and therapeutic efficacy, and toxicity, which could lead to earlier detection and better control of cancer. [91] In development of nanoparticle-based agents for cancer diagnosis and therapy, important factors are active targeting of biomarkers expressed in the tumor and harnessing the enhanced permeability and retention (EPR) effect due to the leaky neovasculature of the tumor proposed by Matsumura and Maeda [92] that can be used for "passive targeting". [93] Compared with conventional small molecule-based anticancer drugs, macromolecules display superior *in vivo* pharmacokinetics and greater tumor delivery and selectivity. [23, 93] Interestingly, a size relationship with the EPR effect was observed that larger and long-circulating macromolecules (> 30–45 kDa) are retained in the tumor tissue longer, whereas smaller molecules easily diffuse back out into the bloodstream. [92] Nanoparticle size, surface modification, and vascular mediators all have been studied as approaches to harness the EPR effect for improved tumor diagnosis and therapy using nanoparticles. [93, 94]

While the EPR effect is helpful, nanoparticles also offer the ability to specifically target tumors based on an individual patient's biology by targeting various biomarkers on the cancer cells. To date, a range of targeting groups have been developed and used for cancer nanomedicine. [3, 95–99] Among them, antisense-based imaging agents such as phosphodiester (PO) oligodeoxynucleotides (ODN) and phosphorothioate (PS)-ODNs, which are designed according to the gene expression profile of human cancerous cells, are promising imaging probes for the early and specific detection of cancer due to the high specificity. [100] However, the rapid degradation by endo- and exonucleases *in vivo* made their PET imaging challenging. Alternatively, with the complete replacement of the sugar-phosphate backbone to amine backbone (peptide nucleic acids or PNA) through chemical modification, the PNAs displayed strong resistance to enzymatic degradation without changing the binding affinity and specificity. Therefore, a specially designed PNA sequence was used to target the elevated expression of upstream of N-ras (unr) mRNA in a mouse MCF-7 breast tumor model with $^{64}$Cu radiolabeling. PET imaging clearly showed the tumor accumulation of $^{64}$Cu-DOTA-PNA50-K4, indicating the potential of this antisense PNA as a specific molecular probe for cancer diagnosis. [101] Thus, this antisense PNA (PNA50) was conjugated to well-defined SCK nanoparticles for further evaluation. The *in vivo* pharmacokinetic studies demonstrated improved biodistribution profiles relative to PNA alone tracer while maintaining the PNA binding capability to target, indicating the potential of this nanoprobe for sensitive and specific cancer diagnosis. [102]

In another study, SCKs conjugated with folate showed specific interaction with folate receptors overexpressed in KB cells. *In vivo* studies with $^{64}$Cu labeling demonstrated improved blood retention and folate receptor-mediated uptake of SCKs in small tumors. [103] To develop sensitive nanoprobes for cancer diagnosis, the click chemistry strategy has also been explored on SCKs to obtain ultrahigh specific activity $^{64}$Cu/$^{18}$F radiolabeled nanoparticles as well as controlled conjugation of targeting ligands by designing click sites both in the core and on the surface. [104, 105]

Iron oxide nanoparticles have been widely explored for PET/MR or PET/MR/optical tumor imaging. [106–108] With optimized surface pegylation and DOTA functionalization, a $^{64}$Cu radiolabeled iron oxide nanoparticle (specific activity = 3.7–7.4×10$^8$ Bq/mg Fe) showed elevated blood retention of 37.3± 12.9 %ID/g at 1h post injection in mice, confirmed by

PET imaging (Figure 6). In another study, a cyclic RGD peptide (c(RGDfC)) was conjugated to a superparamagnetic iron oxide nanoparticle (SPIO) for targeted PET/MR tumor imaging. [109, 110] This $^{64}$Cu-cRGD-SPIO illustrated low (<15 %ID/g) hepatic burden up to 48h and constant tumor uptake (~5% ID/g) across the study with the highest (11.3±2.5) tumor/muscle ratio observed at 48h. Furthermore, compared to the control $^{64}$Cu-SPIO, $^{64}$Cu-cRGD-SPIO had significantly ($p<0.05$) higher tumor accumulation during the study, indicating $\alpha_v\beta_3$-specific targeting.[40]

Lately, Cerenkov luminescence imaging has become an active topic in biomedical research due to the combination of nuclear tomography with optical techniques generated from the decay of radionuclides, and suitability for the rapid, high-throughput screening. [111] Thus, a $^{124}$I radiolabeled iron oxide nanoparticle was developed for optical/PET/MR tri-modality tumor imaging. The complementary nature of this hybrid nanoprobe facilitated non-invasive differentiation between tumor-metastasized sentinel lymph nodes (SLNs) and tumor-free SLNs.[112]

Silica nanoparticles, which are inherently nontoxic and biocompatible, have been an attractive candidate for theranostics in various patient settings. With cRGDY conjugation, high *in vitro* binding affinity ($IC_{50}$ = 1.2 nM) was achieved. In animal melanoma model, this targeted $^{124}$I-cRGDY-PEG-dots nanoprobe showed optimized pharmacokinetics (blood and tumor half-lives = 5.9 hours and 73.5 hours, respectively), $\alpha_v\beta_3$-specific tumor uptake, and high tumor-to-muscle ratio (T/M=5 at 24h). Dosimetry studies demonstrated comparable radiation doses to other clinically used PET tracers. Toxicity studies confirmed full clearance in one week and no tissue-specific pathologic effect. Therefore, a human clinical trial has been planned to investigate the potential of this targeted nanoprobe in staging metastatic disease in the clinical setting. [24]

Another effort to develop theranostic agents involves use of various gold nanostructures such as nanoparticles, nanorods, nanoshells, and nanocages due to the well-known biocompatibility. They can serve as optical imaging agents due to the surface plasmon resonance, or PET imaging probe through surface conjugation. More importantly, their photothermal properties empower the conversion of absorbed light into heat through nonradiative electron relaxation dynamics for cancer treatment. [9, 43] Thus, gold nanoshell was used for multimodality theranostics with $^{64}$Cu radiolabeling and RGD peptide conjugation. PET/CT of this $^{64}$Cu-NS-RGDfK showed significant tumor uptake and tumor vascular specificity, indicating the active targeting and improved efficacy of photothermal ablation. [113] Additionally, a chelator-free [$^{64}$Cu]CuS nanoparticle with controlled specific activity was also prepared for tumor theranostic application. The pegylated [$^{64}$Cu]CuS nanoparticles showed about 15% ID/g blood retention at 4h in biodistribution studies and high tumor-to-muscle ratio (T/M=6.55) at 24h. Interestingly, this PEG-[$^{64}$Cu]CuS nanoparticle also displayed the photothermal property. [114]

Liposomes, widely used for drug delivery in both clinical and pre-clinical applications, [115] can also be a good theranostic candidate. [116] Initially, liposomes with $^{64}$Cu radiolabeling have been used to probe the EPR effect in tumor-bearing mice. With a remote loading approach for $^{64}$Cu encapsulation, improved radiolabeling stability and tumor accumulation ((5.0 ± 2.0% ID/organ) was obtained, confirmed by PET/CT. [117] This approach was used to study the EPR effect during the transition from premalignant to malignant cancer in a mouse ductal carcinoma model. With disease progression, the vascular volume fraction increased 1.6-fold and the apparent vascular permeability to liposomes increased about 2.5-fold. Thanks to the long *in vivo* half-life ($t_{1/2}$=18h), high tumor/muscle ratio (17.9±8.1) was achieved with $^{64}$Cu-liposomes. Interestingly, more heterogeneous intratumoral distribution was observed in the presence of increased vascular permeability. [118] More importantly, by

adding encapsulation of EGFR kinase-targeting group SKI212243, this targeted liposome showed significantly higher tumor accumulation at 48h relative to $^{124}$I-SKI212243 alone and greatly improved tumor-to-background contrast ratio at 48h, indicating specific targeting (not just the EPR effect due to improved circulation). [119]

Lately, with improvement of nanoparticle *in vivo* pharmacokinetics, use of $^{89}$Zr for nanoparticle PET oncological imaging has gained interest owing to its noteworthy physical properties, including long half-life ($t_{1/2}$=78.4h) and high specific activity. [120] In an LS174T colon carcinoma model, the $^{89}$Zr-labeled single wall carbon nanotubes (SWCNT-([$^{89}$Zr]DFO)(E4G10) showed rapid tumor accumulation and gradually increased tumor-to-muscle contrast ratio over time (1.61 at 1h to 5.08 at 96h). In another colon carcinoma model (CT26), an $^{89}$Zr-labeled cross-linked dextran nanoparticle showed primary localization in lymph node (34 ± 16%ID/g). In some tumor bearing mice, PET imaging showed intense tumor uptake (20 ± 5%ID/g), surprisingly higher than other MPS organs, indicating translational potential. [121]

## CONCLUSION

A variety of nanoparticles has been engineered and explored for diagnostic and therapeutic potential in various diseases. The examples presented in this review focus on nanoparticles labeled with PET isotopes for cardiovascular, pulmonary and tumor imaging, as well as for pharmacokinetic evaluation. So far, significant progress has been achieved in nanoparticle structure design, *in vitro* trafficking, and *in vivo* fate mapping by using PET. More effort will be necessary to achieve active targeting and quantification of low level biomarkers expressed in animal models using customized nanoparticles generated through new chemistry for early disease detection and prevention with PET, and to achieve development of approved biocompatible and biodegradable nanoparticles for personalized medicine and translational research.

## Acknowledgments

The authors' work presented is supported by the National Heart, Lung and Blood Institute of the National Institutes of Health as a Program of Excellence in Nanotechnology (HHSN268201000046C).

## LITERATURE CITED

1. Schober O, Rahbar K, Riemann B. Multimodality molecular imaging--from target description to clinical studies. Eur J Nucl Med Mol Imaging. 2009; 36:302–14. [PubMed: 19130054]
2. Hagooly A, Rossin R, Welch MJ. Small molecule receptors as imaging targets. Handb Exp Pharmacol. 2008:93–129. [PubMed: 18626600]
3. Gunasekera UA, Pankhurst QA, Douek M. Imaging applications of nanotechnology in cancer. Target Oncol. 2009; 4:169–81. [PubMed: 19876702]
4. Sanvicens N, Marco MP. Multifunctional nanoparticles--properties and prospects for their use in human medicine. Trends Biotechnol. 2008; 26:425–33. [PubMed: 18514941]
5. Liu Z, Cai W, He L, Nakayama N, Chen K, Sun X, Chen X, Dai H. In vivo biodistribution and highly efficient tumour targeting of carbon nanotubes in mice. Nat Nanotechnol. 2007; 2:47–52. [PubMed: 18654207]
6. Villa CH, McDevitt MR, Escorcia FE, Rey DA, Bergkvist M, Batt CA, Scheinberg DA. Synthesis and biodistribution of oligonucleotide-functionalized, tumor-targetable carbon nanotubes. Nano Lett. 2008; 8:4221–8. [PubMed: 19367842]
7. Rojas S, Gispert JD, Martin R, Abad S, Menchon C, Pareto D, Victor VM, Alvaro M, Garcia H, Herance JR. Biodistribution of Amino-Functionalized Diamond Nanoparticles. In Vivo Studies Based on (18)F Radionuclide Emission. ACS Nano. 2011; 5:5552–5559. [PubMed: 21657210]

8. McDevitt MR, Chattopadhyay D, Jaggi JS, Finn RD, Zanzonico PB, Villa C, Rey D, Mendenhall J, Batt CA, Njardarson JT, Scheinberg DA. PET imaging of soluble yttrium-86-labeled carbon nanotubes in mice. PLoS One. 2007; 2:e907. [PubMed: 17878942]
9. Khlebtsov N, Dykman L. Biodistribution and toxicity of engineered gold nanoparticles: a review of in vitro and in vivo studies. Chem Soc Rev. 2011; 40:1647–71. [PubMed: 21082078]
10. Li SD, Huang L. Pharmacokinetics and biodistribution of nanoparticles. Mol Pharm. 2008; 5:496–504. [PubMed: 18611037]
11. Owens DE 3rd, Peppas NA. Opsonization, biodistribution, and pharmacokinetics of polymeric nanoparticles. Int J Pharm. 2006; 307:93–102. [PubMed: 16303268]
12. Cormode DP, Skajaa T, Fayad ZA, Mulder WJ. Nanotechnology in medical imaging: probe design and applications. Arterioscler Thromb Vasc Biol. 2009; 29:992–1000. [PubMed: 19057023]
13. Schipper ML, Cheng Z, Lee SW, Bentolila LA, Iyer G, Rao J, Chen X, Wu AM, Weiss S, Gambhir SS. microPET-based biodistribution of quantum dots in living mice. J Nucl Med. 2007; 48:1511–8. [PubMed: 17704240]
14. Zhang JS, Liu F, Huang L. Implications of pharmacokinetic behavior of lipoplex for its inflammatory toxicity. Adv Drug Deliv Rev. 2005; 57:689–98. [PubMed: 15757755]
15. Jokerst JV, Lobovkina T, Zare RN, Gambhir SS. Nanoparticle PEGylation for imaging and therapy. Nanomedicine (Lond). 2011; 6:715–28. [PubMed: 21718180]
16. Jarzyna PA, Gianella A, Skajaa T, Knudsen G, Deddens LH, Cormode DP, Fayad ZA, Mulder WJ. Multifunctional imaging nanoprobes. Wiley Interdiscip Rev Nanomed Nanobiotechnol. 2010; 2:138–50. [PubMed: 20039335]
17. Welch MJ, Hawker CJ, Wooley KL. The advantages of nanoparticles for PET. J Nucl Med. 2009; 50:1743–6. [PubMed: 19837751]
18. Minchin RF, Martin DJ. Nanoparticles for molecular imaging--an overview. Endocrinology. 2010; 151:474–81. [PubMed: 20016027]
19. Loudos G, Kagadis GC, Psimadas D. Current status and future perspectives of in vivo small animal imaging using radiolabeled nanoparticles. Eur J Radiol. 2010; 78:287–295. [PubMed: 20637553]
20. Hong H, Zhang Y, Sun J, Cai W. Molecular imaging and therapy of cancer with radiolabeled nanoparticles. Nano Today. 2009; 4:399–413. [PubMed: 20161038]
21. Gomes CM, Abrunhosa AJ, Ramos P, Pauwels EK. Molecular imaging with SPECT as a tool for drug development. Adv Drug Deliv Rev. 2011; 63:547–54. [PubMed: 20933557]
22. Heidel JD, Davis ME. Clinical developments in nanotechnology for cancer therapy. Pharm Res. 2011; 28:187–99. [PubMed: 20549313]
23. Schluep T, Hwang J, Hildebrandt IJ, Czernin J, Choi CH, Alabi CA, Mack BC, Davis ME. Pharmacokinetics and tumor dynamics of the nanoparticle IT-101 from PET imaging and tumor histological measurements. Proc Natl Acad Sci U S A. 2009; 106:11394–9. [PubMed: 19564622]
24. Benezra M, Penate-Medina O, Zanzonico PB, Schaer D, Ow H, Burns A, Destanchina E, Longo V, Herz E, Iyer S, Wolchok J, Larson SM, Wiesner U, Bradbury MS. Multimodal silica nanoparticles are effective cancer-targeted probes in a model of human melanoma. J Clin Invest. 2011; 121:2768–80. [PubMed: 21670497]
25. Ray P. The pivotal role of multimodality reporter sensors in drug discovery: from cell based assays to real time molecular imaging. Curr Pharm Biotechnol. 2011; 12:539–46. [PubMed: 21342103]
26. Glaus C, Rossin R, Welch MJ, Bao G. In vivo evaluation of (64)Cu-labeled magnetic nanoparticles as a dual-modality PET/MR imaging agent. Bioconjug Chem. 2010; 21:715–22. [PubMed: 20353170]
27. Almutairi A, Rossin R, Shokeen M, Hagooly A, Ananth A, Capoccia B, Guillaudeu S, Abendschein D, Anderson CJ, Welch MJ, Frechet JM. Biodegradable dendritic positron-emitting nanoprobes for the noninvasive imaging of angiogenesis. Proc Natl Acad Sci U S A. 2009; 106:685–90. [PubMed: 19129498]
28. Rossin R, Muro S, Welch MJ, Muzykantov VR, Schuster DP. In vivo imaging of 64Cu-labeled polymer nanoparticles targeted to the lung endothelium. J Nucl Med. 2008; 49:103–11. [PubMed: 18077519]

29. Liu Y, Ibricevic A, Cohen JA, Cohen JL, Gunsten SP, Frechet JM, Walter MJ, Welch MJ, Brody SL. Impact of hydrogel nanoparticle size and functionalization on in vivo behavior for lung imaging and therapeutics. Mol Pharm. 2009; 6:1891–902. [PubMed: 19852512]
30. Tang L. Radionuclide production and yields at Washington University School of Medicine. Q J Nucl Med Mol Imaging. 2008; 52:121–33. [PubMed: 18043542]
31. Hamoudeh M, Kamleh MA, Diab R, Fessi H. Radionuclides delivery systems for nuclear imaging and radiotherapy of cancer. Adv Drug Deliv Rev. 2008; 60:1329–46. [PubMed: 18562040]
32. Shokeen M, Fettig NM, Rossin R. Synthesis, in vitro and in vivo evaluation of radiolabeled nanoparticles. Q J Nucl Med Mol Imaging. 2008; 52:267–77. [PubMed: 18475250]
33. Kagadis GC, Loudos G, Katsanos K, Langer SG, Nikiforidis GC. In vivo small animal imaging: current status and future prospects. Med Phys. 2010; 37:6421–42. [PubMed: 21302799]
34. Anderson CJ, Ferdani R. Copper-64 radiopharmaceuticals for PET imaging of cancer: advances in preclinical and clinical research. Cancer Biother Radiopharm. 2009; 24:379–93. [PubMed: 19694573]
35. http://clinicaltrials.gov/ct2/results?term=dota.
36. Schipper ML, Iyer G, Koh AL, Cheng Z, Ebenstein Y, Aharoni A, Keren S, Bentolila LA, Li J, Rao J, Chen X, Banin U, Wu AM, Sinclair R, Weiss S, Gambhir SS. Particle size, surface coating, and PEGylation influence the biodistribution of quantum dots in living mice. Small. 2009; 5:126–34. [PubMed: 19051182]
37. Hardman R. A toxicologic review of quantum dots: toxicity depends on physicochemical and environmental factors. Environ Health Perspect. 2006; 114:165–72. [PubMed: 16451849]
38. McCarthy JR, Weissleder R. Multifunctional magnetic nanoparticles for targeted imaging and therapy. Adv Drug Deliv Rev. 2008; 60:1241–51. [PubMed: 18508157]
39. Heesakkers RA, Hovels AM, Jager GJ, van den Bosch HC, Witjes JA, Raat HP, Severens JL, Adang EM, van der Kaa CH, Futterer JJ, Barentsz J. MRI with a lymph-node-specific contrast agent as an alternative to CT scan and lymph-node dissection in patients with prostate cancer: a prospective multicohort study. Lancet Oncol. 2008; 9:850–6. [PubMed: 18708295]
40. Yang X, Hong H, Grailer JJ, Rowland IJ, Javadi A, Hurley SA, Xiao Y, Yang Y, Zhang Y, Nickles RJ, Cai W, Steeber DA, Gong S. cRGD-functionalized, DOX-conjugated, and (64)Cu-labeled superparamagnetic iron oxide nanoparticles for targeted anticancer drug delivery and PET/MR imaging. Biomaterials. 2011; 32:4151–60. [PubMed: 21367450]
41. Stelter L, Pinkernelle JG, Michel R, Schwartlander R, Raschzok N, Morgul MH, Koch M, Denecke T, Ruf J, Baumler H, Jordan A, Hamm B, Sauer IM, Teichgraber U. Modification of aminosilanized superparamagnetic nanoparticles: feasibility of multimodal detection using 3T MRI, small animal PET, and fluorescence imaging. Mol Imaging Biol. 2010; 12:25–34. [PubMed: 19582510]
42. Choi JS, Park JC, Nah H, Woo S, Oh J, Kim KM, Cheon GJ, Chang Y, Yoo J, Cheon J. A hybrid nanoparticle probe for dual-modality positron emission tomography and magnetic resonance imaging. Angew Chem Int Ed Engl. 2008; 47:6259–62. [PubMed: 18613191]
43. Chen J, Glaus C, Laforest R, Zhang Q, Yang M, Gidding M, Welch MJ, Xia Y. Gold nanocages as photothermal transducers for cancer treatment. Small. 2010; 6:811–7. [PubMed: 20225187]
44. Xie H, Wang ZJ, Bao A, Goins B, Phillips WT. In vivo PET imaging and biodistribution of radiolabeled gold nanoshells in rats with tumor xenografts. Int J Pharm. 2010; 395:324–30. [PubMed: 20540999]
45. Gregoriadis G, Ryman BE. Liposomes as carriers of enzymes or drugs: a new approach to the treatment of storage diseases. Biochem J. 1971; 124:58P.
46. Phillips WT, Goins BA, Bao A. Radioactive liposomes. Wiley Interdiscip Rev Nanomed Nanobiotechnol. 2009; 1:69–83. [PubMed: 20049780]
47. Bimbo LM, Sarparanta M, Santos HA, Airaksinen AJ, Makila E, Laaksonen T, Peltonen L, Lehto VP, Hirvonen J, Salonen J. Biocompatibility of thermally hydrocarbonized porous silicon nanoparticles and their biodistribution in rats. ACS Nano. 2010; 4:3023–32. [PubMed: 20509673]
48. Kumar R, Roy I, Ohulchanskky TY, Vathy LA, Bergey EJ, Sajjad M, Prasad PN. In vivo biodistribution and clearance studies using multimodal organically modified silica nanoparticles. ACS Nano. 2010; 4:699–708. [PubMed: 20088598]

49. Martin R, Menchon C, Apostolova N, Victor VM, Alvaro M, Herance JR, Garcia H. Nano-jewels in biology. Gold and platinum on diamond nanoparticles as antioxidant systems against cellular oxidative stress. ACS Nano. 2010; 4:6957–65. [PubMed: 20939514]
50. Liu Q, Sun Y, Li C, Zhou J, Li C, Yang T, Zhang X, Yi T, Wu D, Li F. 18F-Labeled magnetic-upconversion nanophosphors via rare-Earth cation-assisted ligand assembly. ACS Nano. 2011; 5:3146–57. [PubMed: 21384900]
51. Zhou J, Yu M, Sun Y, Zhang X, Zhu X, Wu Z, Wu D, Li F. Fluorine-18-labeled Gd3+/Yb3+/Er3+ co-doped NaYF4 nanophosphors for multimodality PET/MR/UCL imaging. Biomaterials. 2011; 32:1148–56. [PubMed: 20965563]
52. Sun Y, Yu M, Liang S, Zhang Y, Li C, Mou T, Yang W, Zhang X, Li B, Huang C, Li F. Fluorine-18 labeled rare-earth nanoparticles for positron emission tomography (PET) imaging of sentinel lymph node. Biomaterials. 2011; 32:2999–3007. [PubMed: 21295345]
53. Buxton DB. Nanotechnology research support at the national heart, lung, and blood institute. Circ Res. 2011; 109:250–4. [PubMed: 21778434]
54. Sun G, Hagooly A, Xu J, Nystrom AM, Li Z, Rossin R, Moore DA, Wooley KL, Welch MJ. Facile, efficient approach to accomplish tunable chemistries and variable biodistributions for shell cross-linked nanoparticles. Biomacromolecules. 2008; 9:1997–2006. [PubMed: 18510359]
55. Nahrendorf M, Sosnovik DE, French BA, Swirski FK, Bengel F, Sadeghi MM, Lindner JR, Wu JC, Kraitchman DL, Fayad ZA, Sinusas AJ. Multimodality cardiovascular molecular imaging, Part II. Circ Cardiovasc Imaging. 2009; 2:56–70. [PubMed: 19808565]
56. Sinusas AJ, Bengel F, Nahrendorf M, Epstein FH, Wu JC, Villanueva FS, Fayad ZA, Gropler RJ. Multimodality cardiovascular molecular imaging, part I. Circ Cardiovasc Imaging. 2008; 1:244–56. [PubMed: 19808549]
57. Nahrendorf M, Zhang H, Hembrador S, Panizzi P, Sosnovik DE, Aikawa E, Libby P, Swirski FK, Weissleder R. Nanoparticle PET-CT imaging of macrophages in inflammatory atherosclerosis. Circulation. 2008; 117:379–87. [PubMed: 18158358]
58. Buxton DB. Current status of nanotechnology approaches for cardiovascular disease: a personal perspective. Wiley Interdiscip Rev Nanomed Nanobiotechnol. 2009; 1:149–55. [PubMed: 20049786]
59. Anderson CJ, Bulte JW, Chen K, Chen X, Khaw BA, Shokeen M, Wooley KL, VanBrocklin HF. Design of targeted cardiovascular molecular imaging probes. J Nucl Med. 2010; 51(Suppl 1):3S–17S. [PubMed: 20395345]
60. Gaucher G, Dufresne MH, Sant VP, Kang N, Maysinger D, Leroux JC. Block copolymer micelles: preparation, characterization and application in drug delivery. J Control Release. 2005; 109:169–88. [PubMed: 16289422]
61. Nishiyama N, Kataoka K. Current state, achievements, and future prospects of polymeric micelles as nanocarriers for drug and gene delivery. Pharmacol Ther. 2006; 112:630–48. [PubMed: 16815554]
62. Xu J, Sun G, Rossin R, Hagooly A, Li Z, Fukukawa KI, Messmore BW, Moore DA, Welch MJ, Hawker CJ, Wooley KL. Labeling of Polymer Nanostructures for Medical Imaging: Importance of crosslinking extent, spacer length, and charge density. Macromolecules. 2007; 40:2971–2973. [PubMed: 18779874]
63. Sun G, Xu J, Hagooly A, Rossin R, Li Z, Moore DA, Hawker CJ, Welch MJ, Wooley KL. Strategies for Optimized Radiolabeling of Nanoparticles for in vivo PET Imaging. Advanced Materials. 2007; 19:3157–3162.
64. Fukukawa K, Rossin R, Hagooly A, Pressly ED, Hunt JN, Messmore BW, Wooley KL, Welch MJ, Hawker CJ. Synthesis and characterization of core-shell star copolymers for in vivo PET imaging applications. Biomacromolecules. 2008; 9:1329–39. [PubMed: 18338840]
65. Pressly ED, Rossin R, Hagooly A, Fukukawa K, Messmore BW, Welch MJ, Wooley KL, Lamm MS, Hule RA, Pochan DJ, Hawker CJ. Structural effects on the biodistribution and positron emission tomography (PET) imaging of well-defined (64)Cu-labeled nanoparticles comprised of amphiphilic block graft copolymers. Biomacromolecules. 2007; 8:3126–34. [PubMed: 17880180]

66. Shokeen M, Pressly ED, Hagooly A, Zheleznyak A, Ramos N, Fiamengo AL, Welch MJ, Hawker CJ, Anderson CJ. Evaluation of multivalent, functional polymeric nanoparticles for imaging applications. ACS Nano. 2011; 5:738–47. [PubMed: 21275414]

67. Liu Y, Pressly ED, Abendschein D, Hawker CJ, Woodard GE, Woodard PK, Welch MJ. Targeting angiogenesis using a C-type atrial natriuretic factor conjugated nanoprobe and positron emission tomography. Journal of Nuclear Medicine. 2011; 52:1956–1963. [PubMed: 22049461]

68. Kumari A, Yadav SK, Yadav SC. Biodegradable polymeric nanoparticles based drug delivery systems. Colloids Surf B Biointerfaces. 2010; 75:1–18. [PubMed: 19782542]

69. Soppimath KS, Aminabhavi TM, Kulkarni AR, Rudzinski WE. Biodegradable polymeric nanoparticles as drug delivery devices. J Control Release. 2001; 70:1–20. [PubMed: 11166403]

70. Gan CW, Chien S, Feng SS. Nanomedicine: enhancement of chemotherapeutical efficacy of docetaxel by using a biodegradable nanoparticle formulation. Curr Pharm Des. 2010; 16:2308–20. [PubMed: 20618152]

71. Courant T, Roullin VG, Cadiou C, Delavoie F, Molinari M, Andry MC, Chuburu F. Development and physicochemical characterization of copper complexes-loaded PLGA nanoparticles. Int J Pharm. 2009; 379:226–34. [PubMed: 19428198]

72. Devaraj NK, Keliher EJ, Thurber GM, Nahrendorf M, Weissleder R. 18F labeled nanoparticles for in vivo PET-CT imaging. Bioconjug Chem. 2009; 20:397–401. [PubMed: 19138113]

73. Nahrendorf M, Keliher E, Marinelli B, Leuschner F, Robbins CS, Gerszten RE, Pittet MJ, Swirski FK, Weissleder R. Detection of macrophages in aortic aneurysms by nanoparticle positron emission tomography-computed tomography. Arterioscler Thromb Vasc Biol. 2011; 31:750–7. [PubMed: 21252070]

74. Swai H, Semete B, Kalombo L, Chelule P, Kisich K, Sievers B. Nanomedicine for respiratory diseases. Wiley Interdiscip Rev Nanomed Nanobiotechnol. 2009; 1:255–63. [PubMed: 20049795]

75. Rytting E, Nguyen J, Wang X, Kissel T. Biodegradable polymeric nanocarriers for pulmonary drug delivery. Expert Opin Drug Deliv. 2008; 5:629–39. [PubMed: 18532919]

76. Roy I, Vij N. Nanodelivery in airway diseases: challenges and therapeutic applications. Nanomedicine. 2010; 6:237–44. [PubMed: 19616124]

77. Roller J, Laschke MW, Tschernig T, Schramm R, Veith NT, Thorlacius H, Menger MD. How to detect a dwarf: in vivo imaging of nanoparticles in the lung. Nanomedicine. 2011; 7:753–62. [PubMed: 21419874]

78. Card JW, Zeldin DC, Bonner JC, Nestmann ER. Pulmonary applications and toxicity of engineered nanoparticles. Am J Physiol Lung Cell Mol Physiol. 2008; 295:L400–11. [PubMed: 18641236]

79. Semete B, Booysen LI, Kalombo L, Venter JD, Katata L, Ramalapa B, Verschoor JA, Swai H. In vivo uptake and acute immune response to orally administered chitosan and PEG coated PLGA nanoparticles. Toxicol Appl Pharmacol. 2010; 249:158–65. [PubMed: 20851137]

80. Semete B, Booysen L, Lemmer Y, Kalombo L, Katata L, Verschoor J, Swai HS. In vivo evaluation of the biodistribution and safety of PLGA nanoparticles as drug delivery systems. Nanomedicine. 2010; 6:662–71. [PubMed: 20230912]

81. Murthy N, Xu M, Schuck S, Kunisawa J, Shastri N, Frechet JM. A macromolecular delivery vehicle for protein-based vaccines: acid-degradable protein-loaded microgels. Proc Natl Acad Sci U S A. 2003; 100:4995–5000. [PubMed: 12704236]

82. Murthy N, Thng YX, Schuck S, Xu MC, Frechet JM. A novel strategy for encapsulation and release of proteins: hydrogels and microgels with acid-labile acetal cross-linkers. J Am Chem Soc. 2002; 124:12398–9. [PubMed: 12381166]

83. Standley SM, Kwon YJ, Murthy N, Kunisawa J, Shastri N, Guillaudeu SJ, Lau L, Frechet JM. Acid-degradable particles for protein-based vaccines: enhanced survival rate for tumor-challenged mice using ovalbumin model. Bioconjug Chem. 2004; 15:1281–8. [PubMed: 15546194]

84. Lundberg P, Langel U. A brief introduction to cell-penetrating peptides. J Mol Recognit. 2003; 16:227–33. [PubMed: 14523933]

85. Shoyele SA, Cawthorne S. Particle engineering techniques for inhaled biopharmaceuticals. Adv Drug Deliv Rev. 2006; 58:1009–29. [PubMed: 17005293]

86. Cohen JL, Almutairi A, Cohen JA, Bernstein M, Brody SL, Schuster DP, Frechet JM. Enhanced cell penetration of acid-degradable particles functionalized with cell-penetrating peptides. Bioconjug Chem. 2008; 19:876–81. [PubMed: 18318462]
87. Rojas S, Gispert JD, Martin R, Abad S, Menchon C, Pareto D, Victor VM, Alvaro M, Garcia H, Herance JR. Biodistribution of amino-functionalized diamond nanoparticles. In vivo studies based on 18F radionuclide emission. ACS Nano. 2011; 5:5552–9. [PubMed: 21657210]
88. Hofman MS, Beauregard JM, Barber TW, Neels OC, Eu P, Hicks RJ. 68Ga PET/CT ventilation-perfusion imaging for pulmonary embolism: a pilot study with comparison to conventional scintigraphy. J Nucl Med. 2011; 52:1513–9. [PubMed: 21908388]
89. Strebhardt K, Ullrich A. Paul Ehrlich's magic bullet concept: 100 years of progress. Nat Rev Cancer. 2008; 8:473–80. [PubMed: 18469827]
90. Ting G, Chang CH, Wang HE. Cancer nanotargeted radiopharmaceuticals for tumor imaging and therapy. Anticancer Res. 2009; 29:4107–18. [PubMed: 19846958]
91. Ting G, Chang CH, Wang HE, Lee TW. Nanotargeted radionuclides for cancer nuclear imaging and internal radiotherapy. J Biomed Biotechnol. 2010:2010.
92. Pirollo KF, Chang EH. Does a targeting ligand influence nanoparticle tumor localization or uptake? Trends Biotechnol. 2008; 26:552–8. [PubMed: 18722682]
93. Fang J, Nakamura H, Maeda H. The EPR effect: Unique features of tumor blood vessels for drug delivery, factors involved, and limitations and augmentation of the effect. Adv Drug Deliv Rev. 2011; 63:136–51. [PubMed: 20441782]
94. Jiang W, Kim BY, Rutka JT, Chan WC. Nanoparticle-mediated cellular response is size-dependent. Nat Nanotechnol. 2008; 3:145–50. [PubMed: 18654486]
95. Adair JH, Parette MP, Altinoglu EI, Kester M. Nanoparticulate alternatives for drug delivery. ACS Nano. 2010; 4:4967–70. [PubMed: 20873786]
96. Minelli C, Lowe SB, Stevens MM. Engineering nanocomposite materials for cancer therapy. Small. 2010; 6:2336–57. [PubMed: 20878632]
97. Hallaj-Nezhadi S, Lotfipour F, Dass CR. Delivery of nanoparticulate drug delivery systems via the intravenous route for cancer gene therapy. Pharmazie. 2010; 65:855–9. [PubMed: 21284252]
98. Alexis F, Pridgen EM, Langer R, Farokhzad OC. Nanoparticle technologies for cancer therapy. Handb Exp Pharmacol. 2010:55–86. [PubMed: 20217526]
99. Pridgen EM, Langer R, Farokhzad OC. Biodegradable, polymeric nanoparticle delivery systems for cancer therapy. Nanomedicine (Lond). 2007; 2:669–80. [PubMed: 17976029]
100. Younes CK, Boisgard R, Tavitian B. Labelled oligonucleotides as radiopharmaceuticals: pitfalls, problems and perspectives. Curr Pharm Des. 2002; 8:1451–66. [PubMed: 12052206]
101. Sun X, Fang H, Li X, Rossin R, Welch MJ, Taylor JS. MicroPET imaging of MCF-7 tumors in mice via unr mRNA-targeted peptide nucleic acids. Bioconjug Chem. 2005; 16:294–305. [PubMed: 15769082]
102. Rossin, R.; Sun, X.; Fang, H.; Turner, JL.; Li, X.; Wooley, KL.; Taylor, JS.; Welch, MJ. Wiley; Iowa city: 2005. Journal of Labelled Compounds and Radiopharmaceuticals; p. S35
103. Rossin R, Pan D, Qi K, Turner JL, Sun X, Wooley KL, Welch MJ. 64Cu-labeled folate-conjugated shell cross-linked nanoparticles for tumor imaging and radiotherapy: synthesis, radiolabeling, and biologic evaluation. J Nucl Med. 2005; 46:1210–8. [PubMed: 16000291]
104. Zhou D, Zeng D, Lee N, Dence C, Wooley K, Katzenellenbogen J, Welch M. Fluorine-18 radiolabeling of SCK nanoparticles via copper-free click chemistry. J NUCL MED MEETING ABSTRACTS. 2011; 52:569.
105. Zeng D, Lee N, Liu Y, Zhou D, Dence C, Wooley K, Katzenellenbogen J, Welch M. Novel strategy for preparing Cu-64 nanoparticles with ultrahigh specific activity using metal-free click chemistry. J NUCL MED MEETING ABSTRACTS. 2011; 52:576.
106. Xie J, Chen K, Huang J, Lee S, Wang J, Gao J, Li X, Chen X. PET/NIRF/MRI triple functional iron oxide nanoparticles. Biomaterials. 2010; 31:3016–22. [PubMed: 20092887]
107. Torres Martin de Rosales R, Tavare R, Paul RL, Jauregui-Osoro M, Protti A, Glaria A, Varma G, Szanda I, Blower PJ. Synthesis of 64Cu(II)-bis(dithiocarbamatebisphosphonate) and its conjugation with superparamagnetic iron oxide nanoparticles: in vivo evaluation as dual-modality PET-MRI agent. Angew Chem Int Ed Engl. 2011; 50:5509–13. [PubMed: 21544908]

108. Jarrett BR, Gustafsson B, Kukis DL, Louie AY. Synthesis of 64Cu-labeled magnetic nanoparticles for multimodal imaging. Bioconjug Chem. 2008; 19:1496–504. [PubMed: 18578485]
109. Tabatabai G, Tonn JC, Stupp R, Weller M. The Role of Integrins in Glioma Biology and Anti-Glioma Therapies. Curr Pharm Des. 2011
110. Beer AJ, Kessler H, Wester HJ, Schwaiger M. PET Imaging of Integrin alphaVbeta3 Expression. Theranostics. 2011; 1:48–57. [PubMed: 21547152]
111. Ruggiero A, Holland JP, Lewis JS, Grimm J. Cerenkov luminescence imaging of medical isotopes. J Nucl Med. 2010; 51:1123–30. [PubMed: 20554722]
112. Park JC, Yu MK, An GI, Park SI, Oh J, Kim HJ, Kim JH, Wang EK, Hong IH, Ha YS, Choi TH, Jeong KS, Chang Y, Welch MJ, Jon S, Yoo J. Facile preparation of a hybrid nanoprobe for triple-modality optical/PET/MR imaging. Small. 2010; 6:2863–8. [PubMed: 21104828]
113. Xie H, Diagaradjane P, Deorukhkar AA, Goins B, Bao A, Phillips WT, Wang Z, Schwartz J, Krishnan S. Integrin alphavbeta3-targeted gold nanoshells augment tumor vasculature-specific imaging and therapy. Int J Nanomedicine. 2011; 6:259–69. [PubMed: 21423588]
114. Zhou M, Zhang R, Huang M, Lu W, Song S, Melancon MP, Tian M, Liang D, Li C. A chelator-free multifunctional [64Cu]CuS nanoparticle platform for simultaneous micro-PET/CT imaging and photothermal ablation therapy. J Am Chem Soc. 2010; 132:15351–8. [PubMed: 20942456]
115. Lammers T, Kiessling F, Hennink WE, Storm G. Nanotheranostics and image-guided drug delivery: current concepts and future directions. Mol Pharm. 2010; 7:1899–912. [PubMed: 20822168]
116. Kelkar SS, Reineke TM. Theranostics: Combining Imaging and Therapy. Bioconjug Chem. 2011; 22:1879–903. [PubMed: 21830812]
117. Petersen AL, Binderup T, Rasmussen P, Henriksen JR, Elema DR, Kjaer A, Andresen TL. 64Cu loaded liposomes as positron emission tomography imaging agents. Biomaterials. 2011; 32:2334–41. [PubMed: 21216003]
118. Rygh CB, Qin S, Seo JW, Mahakian LM, Zhang H, Adamson R, Chen JQ, Borowsky AD, Cardiff RD, Reed RK, Curry FR, Ferrara KW. Longitudinal investigation of permeability and distribution of macromolecules in mouse malignant transformation using PET. Clin Cancer Res. 2010; 17:550–9. [PubMed: 21106723]
119. Medina OP, Pillarsetty N, Glekas A, Punzalan B, Longo V, Gonen M, Zanzonico P, Smith-Jones P, Larson SM. Optimizing tumor targeting of the lipophilic EGFR-binding radiotracer SKI 243 using a liposomal nanoparticle delivery system. J Control Release. 2011; 149:292–8. [PubMed: 21047536]
120. Holland JP, Sheh Y, Lewis JS. Standardized methods for the production of high specific-activity zirconium-89. Nucl Med Biol. 2009; 36:729–39. [PubMed: 19720285]
121. Keliher EJ, Yoo J, Nahrendorf M, Lewis JS, Marinelli B, Newton A, Pittet MJ, Weissleder R. (89)Zr-Labeled Dextran Nanoparticles Allow in Vivo Macrophage Imaging. Bioconjug Chem. 2011; 22:2383–9. [PubMed: 22035047]
122. Duconge F, Pons T, Pestourie C, Herin L, Theze B, Gombert K, Mahler B, Hinnen F, Kuhnast B, Dolle F, Dubertret B, Tavitian B. Fluorine-18-labeled phospholipid quantum dot micelles for in vivo multimodal imaging from whole body to cellular scales. Bioconjug Chem. 2008; 19:1921–6. [PubMed: 18754572]
123. Tu C, Ma X, House A, Kauzlarich SM, Louie AY. PET Imaging and Biodistribution of Silicon Quantum Dots in Mice. ACS Medicinal Chemistry Letters. 2011; 2:285–288. [PubMed: 21546997]
124. Hwang D, Ko H, Kim SK, Kim D, Lee D, Kim S. Development of a Quadruple Imaging Modality by Using Nanoparticles. Chemistry - A European Journal. 2009; 15:9387–9393.
125. Jauregui-Osoro M, Williamson PA, Glaria A, Sunassee K, Charoenphun P, Green MA, Mullen GE, Blower PJ. Biocompatible inorganic nanoparticles for [(18)F]-fluoride binding with applications in PET imaging. Dalton Trans. 2011
126. Liu Q, Sun Y, Li C, Zhou J, Yang T, Zhang X, Yi T, Wu D, Li F. (18)F-Labeled Magnetic-Upconversion Nanophosphors via Rare-Earth Cation-Assisted Ligand Assembly. ACS Nano. 2011; 5:3146–57. [PubMed: 21384900]

127. Cartier R, Kaufner L, Paulke BR, Wustneck R, Pietschmann S, Michel R, Bruhn H, Pison U. Latex nanoparticles for multimodal imaging and detection in vivo. Nanotechnology. 2007; 18:195102.

128. Seo JW, Mahakian LM, Kheirolomoom A, Zhang H, Meares CF, Ferdani R, Anderson CJ, Ferrara KW. Liposomal Cu-64 labeling method using bifunctional chelators: poly(ethylene glycol) spacer and chelator effects. Bioconjug Chem. 2010; 21:1206–15. [PubMed: 20568726]

129. Seo JW, Zhang H, Kukis DL, Meares CF, Ferrara KW. A novel method to label preformed liposomes with 64Cu for positron emission tomography (PET) imaging. Bioconjug Chem. 2008; 19:2577–84. [PubMed: 18991368]

130. Oku N, Yamashita M, Katayama Y, Urakami T, Hatanaka K, Shimizu K, Asai T, Tsukada H, Akai S, Kanazawa H. PET imaging of brain cancer with positron emitter-labeled liposomes. Int J Pharm. 2011; 403:170–7. [PubMed: 20934495]

131. Marik J, Tartis MS, Zhang H, Fung JY, Kheirolomoom A, Sutcliffe JL, Ferrara KW. Long-circulating liposomes radiolabeled with [18F]fluorodipalmitin ([18F]FDP). Nucl Med Biol. 2007; 34:165–71. [PubMed: 17307124]

132. Helbok A, Decristoforo C, Dobrozemsky G, Rangger C, Diederen E, Stark B, Prassl R, von Guggenberg E. Radiolabeling of lipid-based nanoparticles for diagnostics and therapeutic applications: a comparison using different radiometals. J Liposome Res. 2009; 20:219–27. [PubMed: 19863193]

133. Andreozzi E, Seo JW, Ferrara K, Louie A. Novel method to label solid lipid nanoparticles with (64)cu for positron emission tomography imaging. Bioconjug Chem. 2011; 22:808–18. [PubMed: 21388194]

134. Herth MM, Barz M, Moderegger D, Allmeroth M, Jahn M, Thews O, Zentel R, Rosch F. Radioactive labeling of defined HPMA-based polymeric structures using [18F]FETos for in vivo imaging by positron emission tomography. Biomacromolecules. 2009; 10:1697–703. [PubMed: 19425549]

135. Ruggiero A, Villa CH, Holland JP, Sprinkle SR, May C, Lewis JS, Scheinberg DA, McDevitt MR. Imaging and treating tumor vasculature with targeted radiolabeled carbon nanotubes. Int J Nanomedicine. 2010; 5:783–802. [PubMed: 21042424]

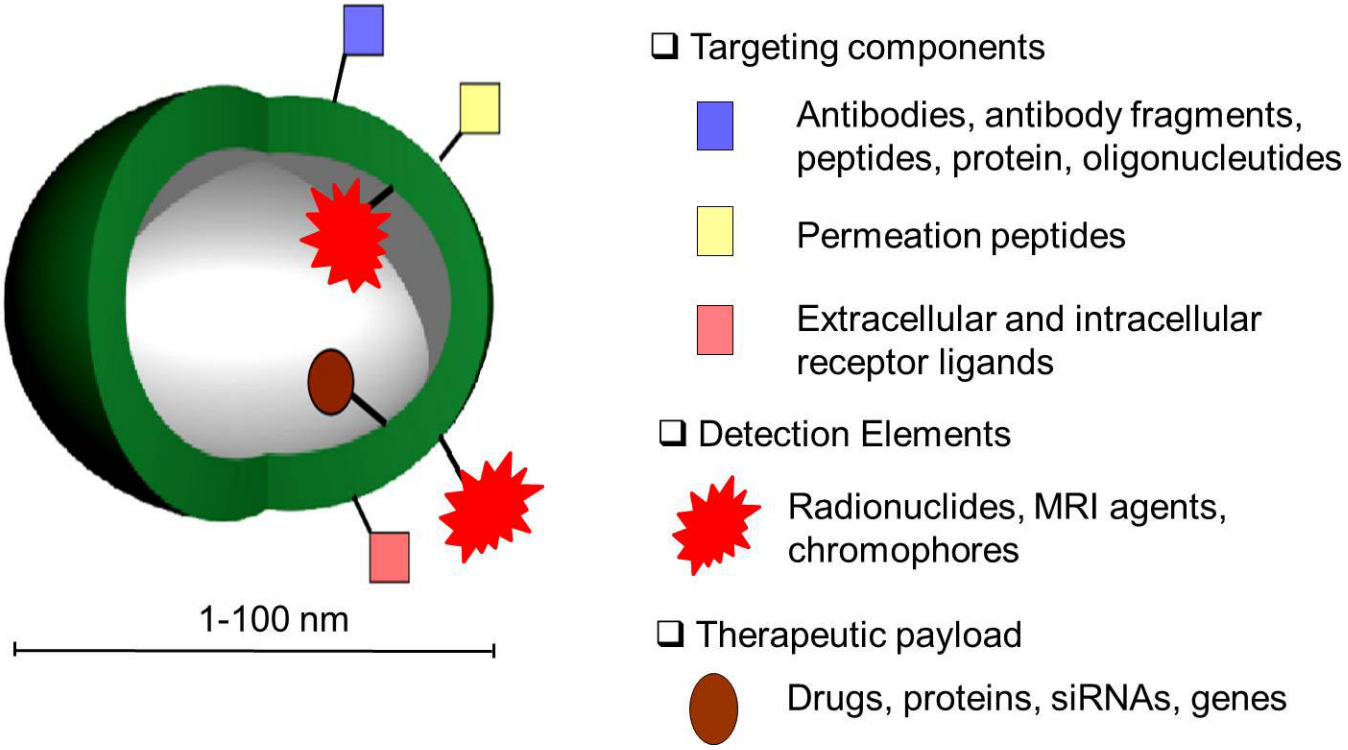


**Figure 1.**
Scheme of multifunctional nanoparticles

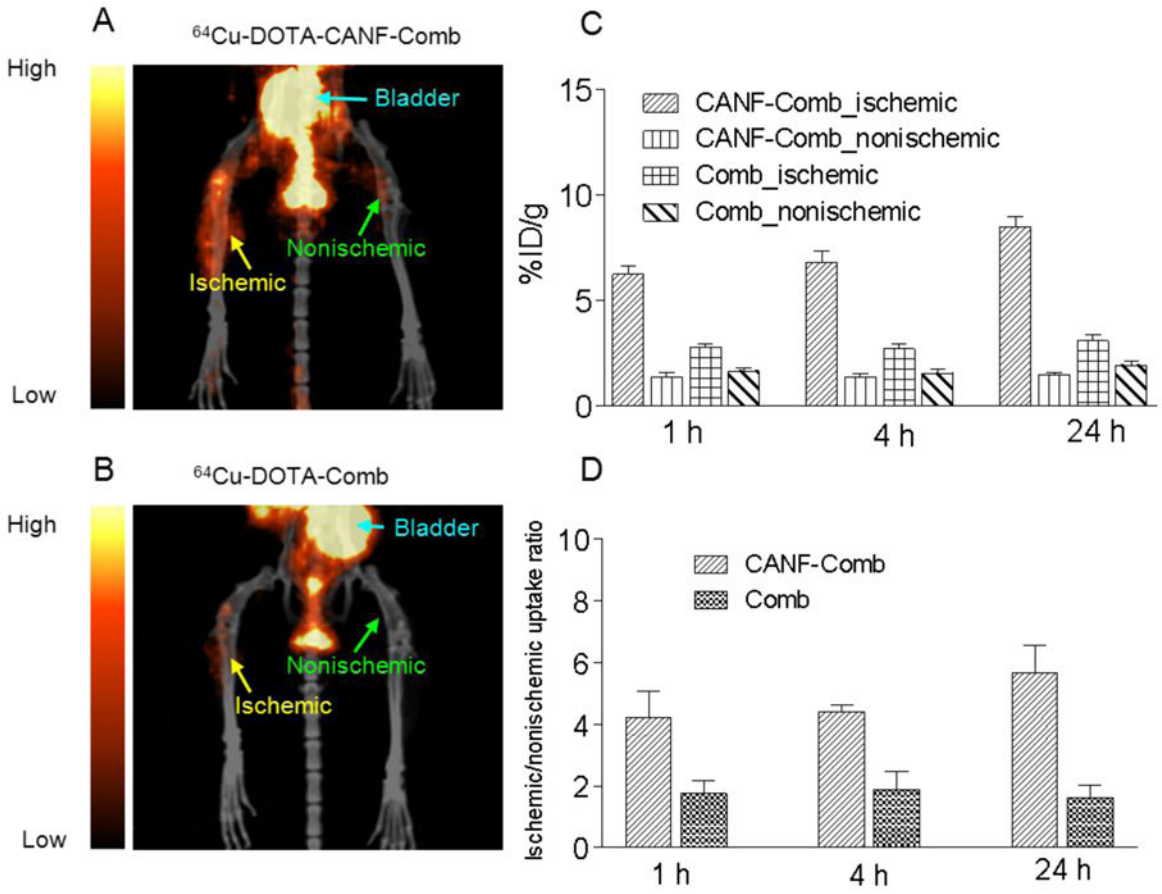


**Figure 2.**

PET/CT images of $^{64}$Cu-DOTA-CANF-Comb and $^{64}$Cu-DOTA-Comb in the HLI induced angiogenesis model obtained 7 days after ischemia. (A) $^{64}$Cu-DOTA-CANF-Comb in HLI model showing the accumulation of activity in the ischemic limb with little observed on the contralateral nonischemic limb. (B) $^{64}$Cu-DOTA-Comb in HLI model showing the weak uptake in both ischemic and nonischemic limbs. (C) Uptake of $^{64}$Cu-DOTA-CANF-Comb (n=8) and $^{64}$Cu-DOTA-Comb (n=7). (D) Ischemic/nonischemic uptake ratios of $^{64}$Cu-DOTA-CANF-Comb (n=8) and $^{64}$Cu-DOTA-Comb (n=7). Figure reproduced with permission from reference 67.

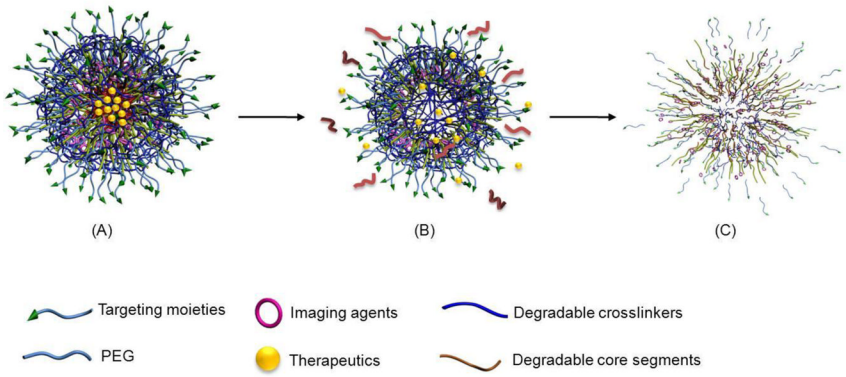


**Figure 3.**
Diagram of the biodegradation process of shell crosslinked knedel-like nanoparticles

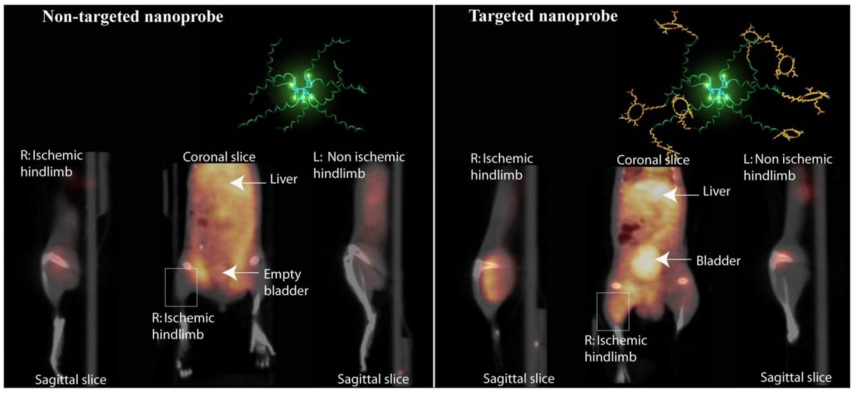


**Figure 4.**

Non-invasive PET/CT images of angiogenesis induced by hindlimb ischemia in a murine model. (A) Nontargeted dendritic nanoprobes (shown bottom center). (B) Uptake of $\alpha_v\beta_3$-targeted dendritic nanoprobes was higher in ischemic hindlimb (left side of image) as compared with control hindlimb (right side of image). Figure reproduced with permission from reference 27.

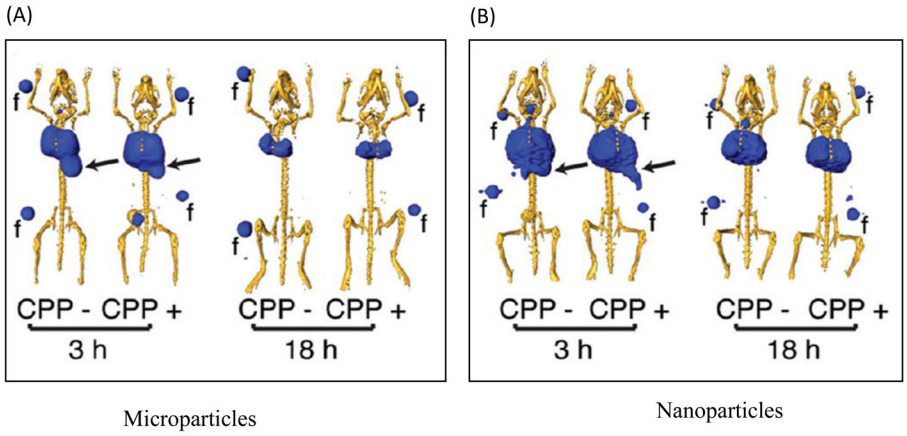


**Figure 5.**

Three dimensional reconstruction of microPET/CT imaging of $^{76}$Br-labeled particles in mice lungs following intratracheal delivery. Arrows indicate gastrointestinal tract activity. Fiduciaries (f) used for coregistration are included. (A) microparticles; (B) nanoparticles. Figure reproduced with permission from reference 29.

CPP−: without cell penetration peptide: CPP+: with cell penetration peptide

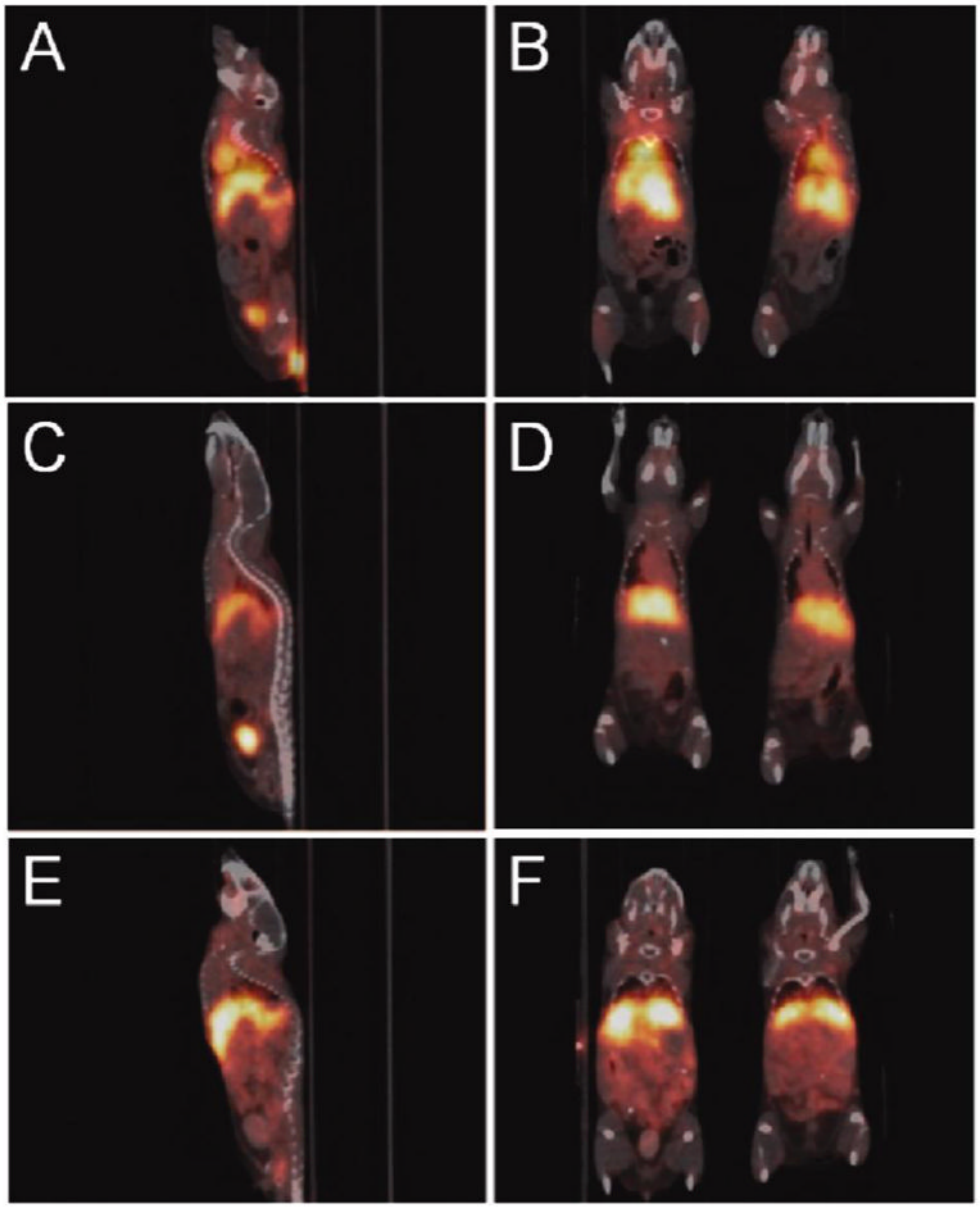


**Figure 6.**
Coregistered microPET/microCT of BALB/c mice administered 100 μCi of $^{64}$Cu-mSPIOs (10 mg Fe/kg body weight, 100 μL injection volume). Whole body sagittal (A-E) and coronal (B-F) PET images are decay corrected and scaled by min/max frame: (A, B) 1 h; (C, D) 4 h; and (E, F) 24 h post injection. Figure reproduced with permission from reference 26.

**Table 1**

Nuclear characteristics of selected PET radionuclides for nanoparticles

| Radionuclide | $T_{1/2}$ | Decay (%) | β Energy (KeV) | | Main photon KeV (%) | Production |
|---|---|---|---|---|---|---|
| | | | Max. | Mean | | |
| $^{68}$Ga | 67.7min | $\beta^+$ (89)<br>EC (11) | 1899 | 829 | 511 (178.3) | $^{68}$Ge/$^{68}$Ga generator |
| $^{18}$F | 109.7min | $\beta^+$ (96.7)<br>EC (0.1) | 634 | 245 | 511 (193.5) | $^{18}$O (p, n) $^{18}$F |
| $^{64}$Cu | 12.7h | $\beta^+$ (17)<br>EC (44) | 653 | 278 | 511 (34.8) | $^{64}$Ni (p, n) $^{64}$Cu |
| $^{76}$Br | 16.2h | $\beta^+$ (55)<br>EC (45) | 3941 | 1180 | 511 (109); 559 (74)<br>657 (15.9); 1854 | $^{76}$Se (p, n) $^{76}$Br<br>$^{76}$Se (d, 2n) $^{76}$Br |
| $^{86}$Y | 14.7h | $\beta^+$ (33)<br>EC (66) | 3141 | 664 | 511 (63.9); 1077 (82.5) | $^{86}$Sr (p, n) $^{86}$Y |
| $^{89}$Zr | 3.3d | $\beta^+$ (23)<br>EC(77) | 901 | 397 | 909 (100) | $^{89}$Y(p, n)$^{89}$Zr |
| $^{124}$I | 4.18d | $\beta^+$ (23)<br>EC (77) | 2138 | 820 | 511 (46); 603 (62.9)<br>723 (10.3) | $^{124}$Te (p, n) $^{124}$I<br>$^{124}$Te (d, 2n) $^{124}$I |

## Table 2

Labeling strategies and specific activities of PET radionuclides labeled nanoparticles

| Nanoparticle | Radionuclide | Labeling strategy | Specific activity* | Reference |
|---|---|---|---|---|
| Quantum dot | $^{18}$F | nucleophilic substitution | 3.7–7.5×10$^8$ Bq (10–20 mCi)/nmol | 122 |
| | $^{64}$Cu | DOTA | 3.7×10$^7$ Bq (1 mCi)/nmol | 36 |
| | $^{64}$Cu | DO3A | 6.2×10$^5$Bq (17μCi)/mg | 123 |
| Iron oxide | $^{18}$F | Click chemistry | 6.7±0.8×10$^8$ Bq (18±2 mCi)/mg Fe | 73 |
| | $^{64}$Cu | DOTA | 3.7–7.4×10$^8$ Bq (10–20 mCi)/mg Fe | 26 |
| | $^{68}$Ga | Direct labeling | 3.6×10$^8$Bq (10 mCi)/nM Fe | 41 |
| | $^{68}$Ga | NOTA | 1.5×10$^8$Bq (4 mCi)/nmol | 124 |
| Aluminum hydroxide | $^{124}$I | Tyrosine | 5.1×10$^7$ Bq (1.4 mCi)/mg (Fe+Mn) | 42 |
| | $^{18}$F | Inorganic interaction | 5.4×10$^6$Bq (146 μCi)/mg | 125 |
| Upconversion nanophosphors | $^{18}$F | Inorganic interaction | 7.8×10$^8$ Bq (21 mCi)/mg | 126 |
| Gold nanoparticle | $^{64}$Cu | DOTA | 5.9×10$^{11}$ Bq (16 Ci)/nmol | 44 |
| Latex | $^{68}$Ga | Direct labeling | 2×10$^5$Bq (5 μCi)/mg | 127 |
| Liposome | $^{64}$Cu | DOTA | 13.3±1.0 ×10$^5$ Bq (36±3 μCi)/nmol | 117 |
| | $^{64}$Cu | TETA, CB-TE2A | 7.7±0.6 ×10$^5$ Bq (21±2 μCi)/nmol | 128 |
| | $^{64}$Cu | BAT | 2.1×10$^7$ Bq (0.6 mCi)/nmol | 129 |
| | $^{18}$F | Encapsulation | 2.8×10$^7$ Bq (0.8 mCi)/nmol | 130 |
| | $^{18}$F | Encapsulation | 1.1×10$^5$ Bq (3 μCi)/nmol | 131 |
| | $^{68}$Ga | DTPA | 4×10$^6$ Bq (0.1 mCi)/μg | 132 |
| Solid lipid nanoparticle | $^{64}$Cu | BAT | 1.4±0.3×10$^6$ Bq (38±8 μCi)/mg lipid | 133 |
| Polymer | $^{76}$Br | Tyrosine | 1.9×10$^5$ Bq (5 μCi)/μg | 27 |
| | $^{64}$Cu | DOTA | 1.5×10$^7$ Bq (0.4 mCi)/μg | 63 |
| | $^{18}$F | [$^{18}$F]FETos | 30 Bq (0.8nCi)/μg | 134 |
| Nanotube | $^{64}$Cu | DOTA | 7.4–11.1×10$^6$ Bq (0.2–0.3 mCi)/μg | 5 |
| | $^{89}$Zr | desferrioxamine B | 592 KBq/μg | 135 |
| | $^{86}$Y | DOTA | 555 GBq/g | 8 |

*The data presented in Table 2 should be reviewed with caution. The values listed in the literature are specific activities quoted during nanoparticle radiolabeling using different units and have also been calculated using different analytical methodologies.